BIOCHEMISTRY

Antiviral activity of a purine synthesis enzyme reveals a key role of deamidation in regulating protein nuclear import

Junhua Li[1]*, Jun Zhao[1], Simin Xu[1], Shu Zhang[1], Junjie Zhang[1], Jun Xiao[1,2], Ruoyun Gao[1], Mao Tian[1], Yi Zeng[1,3], Katie Lee[1], Vera Tarakanova[4], Ke Lan[5], Hao Feng[2], Pinghui Feng[1,5†]

Protein nuclear translocation is highly regulated and crucial for diverse biological processes. However, our understanding concerning protein nuclear import is incomplete. Here we report that a cellular purine synthesis enzyme inhibits protein nuclear import via deamidation. Employing human Kaposi's sarcoma-associated herpesvirus (KSHV) to probe the role of protein deamidation, we identified a purine synthesis enzyme, phosphoribosylformylglycinamidine synthetase (PFAS) that inhibits KSHV transcriptional activation. PFAS deamidates the replication transactivator (RTA), a transcription factor crucial for KSHV lytic replication. Mechanistically, deamidation of two asparagines flanking a positively charged nuclear localization signal impaired the binding of RTA to an importin β subunit, thus diminishing RTA nuclear localization and transcriptional activation. Finally, RTA proteins of all gamma herpesviruses appear to be regulated by PFAS-mediated deamidation. These findings uncover an unexpected function of a metabolic enzyme in restricting viral replication and a key role of deamidation in regulating protein nuclear import.

INTRODUCTION

Functional output of proteins is primarily regulated by a diverse array of posttranslational modifications, such as phosphorylation, ubiquitination, sumoylation, ISGylation, acetylation, methylation, and deamidation (*1*–*4*). Although reported more than half a century ago (*5*), protein deamidation has been largely regarded as a side effect of protein "aging" or functional decay (*6*). Thus, our understanding of protein deamidation is rudimentary at best. Recent studies in microbial infection implicate protein deamidation in regulating host antimicrobial immune responses (*7*–*10*). However, the degree to which protein deamidation regulates fundamental biological processes remains unclear.

Herpesviruses are ubiquitous pathogens in humans. They cause substantial morbidity and mortality worldwide, particularly in immunocompromised individuals. Kaposi's sarcoma–associated herpesvirus (KSHV) is closely related to Epstein-Barr virus (EBV) and induces KS and two rare B cell lymphomas (*11*–*14*). Herpesviruses have evolved elaborate mechanisms to manipulate cellular pathways and establish lifelong persistence within the host, thus offering a robust system to investigate the regulatory mechanism governing fundamental biological processes. We used herpesvirus infection as a model system to probe the role of protein deamidation in virus-host interaction.

Our previous study has shown that gamma herpesviruses deploy viral glutamine amidotransferase (vGAT) pseudoenzymes that recruit cellular phosphoribosylformyl-glycinamidine synthetase (PFAS) to deamidate the RIG-I receptor and block antiviral cytokine production (*9*). PFAS belongs to the GAT family that catalyzes the synthesis of nucleotides, amino acids, glycoproteins, and an enzyme cofactor nicotinamide adenine dinucleotide (NAD) (*15*, *16*). These enzymes contain a signature GAT domain that removes an ammonia group from glutamine and a second catalytic domain that uses ammonia to synthesize the intermediate or final product of the aforementioned anabolic pathways. Our study thus implies that cellular GATs, e.g., PFAS, have intrinsic enzymatic activity to deamidate proteins and regulate signal transduction underlying key biological processes, such as antiviral responses.

RESULTS

Cellular PFAS antagonizes KSHV lytic gene expression

To probe the role of protein deamidation, we carried out a focused screen in which cellular GATs were depleted with short hairpin RNA (shRNA) and KSHV lytic replication was examined. KSHV establishes latent infection by default after de novo infection of most cells. Lytic replication of KSHV can be reactivated from latently infected cells by expressing the replication transactivator (RTA) (*17*). To facilitate KSHV lytic replication, we used rKSHV.219 that expresses green fluorescent protein (GFP) during latent infection, whereas GFP and red fluorescent protein (RFP) are expressed during lytic replication (*18*, *19*). In addition, an inducible 293T cell line that expresses RTA under the control of a doxycycline-responsive promoter (fig. S1A) was established to promote KSHV lytic replication after de novo infection.

The human genome encodes 12 GATs that constitute the putative protein deamidase family. We depleted individual GAT with shRNA in 293T/RTA cells, and KSHV lytic replication was scored by RFP expression (fig. S1A). This focused screen identified five GATs whose knockdown increased KSHV lytic replication (Fig. 1, A and B, and fig. S1B). All five GATs, including PFAS, carbamoyl-phosphate synthetase 2/aspartate transcarbomylase/dihydroorotase (CAD),

[1]Section of Infection and Immunity, Ostrow School of Dentistry, Norris Comprehensive Cancer Center, University of Southern California, 925 W. 34th Street, Los Angeles, CA 90089-0641, USA. [2]Key Laboratory of Protein Chemistry and Developmental Biology of Education Ministry of China, College of Life Sciences, Hunan Normal University, Changsha, Hunan 410081, P.R. China. [3]Department of Pathology and Immunology, Youjiang Medical University for Nationalities, Baise, Guangxi 533000, P.R. China. [4]Department of Microbiology and Immunology, Medical College of Wisconsin, Milwaukee, WI 53226, USA. [5]State Key Laboratory of Virology, Wuhan University, Wuhan, Hubei 430072, P.R. China.
*Present address: State Key Laboratory of Agricultural Microbiology, College of Fisheries, Huazhong Agricultural University, Wuhan, Hubei 430070, P.R. China.
†Corresponding author. Email: pinghui.feng@usc.edu

phosphoribosyl pyrophosphate amidotransferase (PPAT), and cytidine triphosphate (CTP) synthetase 1 (CTPS1) and 2 (CTPS2), catalyze nucleotide synthesis. The knockdown efficiency was validated by real-time polymerase chain reaction (RT-PCR) and immunoblotting analyses (fig. S1, C and D). To alleviate any unintended consequence of GAT depletion, we added the end product of the pathway that each GAT catalyzes (e.g., hypoxanthine for PFAS-depleted cells). GAT depletion did not significantly impair cell survival (fig. S2A). These results show that cellular GATs can inhibit KSHV lytic replication, likely independent of their enzymatic activity in nucleotide synthesis.

Given that RFP in the rKSHV.219 genome is expressed under the control of the RTA-responsive promoter of PAN (*19*), we surmised that GATs may inhibit RTA-mediated transcriptional activation. Reporter assays indicated that PFAS, but not the other four GATs, inhibited the transcription of promoters of PAN and ORF57 in a dose-dependent manner (Fig. 1C and fig. S2B). This result suggests that the other four GATs likely target key processes of KSHV lytic replication other than RTA-mediated transcription. Conversely, knockdown of PFAS increased the transcription of the PAN promoter (Fig. 1D). To further characterize the role of PFAS in KSHV infection, we examined KSHV lytic replication, including gene and protein expression, DNA replication, and extracellular infectious virion production upon PFAS depletion. RT-PCR analysis indicated that PFAS knockdown increased the mRNA levels of KSHV lytic genes, including K8 and PAN (immediately early/early), thymidine kinase (TK; early), and vGAT (late), by a factor of 3 to 5 (Fig. 1E and fig. S2C). Furthermore, PFAS depletion increased RFP expression of rKSHV.219 in iSLK cells (fig. S2D). Immunoblotting analysis validated the elevated levels of viral lytic proteins, including RTA, K3, TK, and vGAT, upon PFAS depletion (Fig. 1F). Last, elevated viral lytic gene expression correlated with a nearly fivefold increase in viral genome copy and extracellular infectious virion particles (Fig. 1, G and H). Human oral keratinocytes (HOKs) were reported to support KSHV lytic replication (*20*, *21*); thus, we examined KSHV lytic replication in HOK cells. PFAS depletion also augmented KSHV lytic replication in HOK cells, as assessed by RFP expression (fig. S2, E and F). Collectively, these results showed that PFAS depletion increased KSHV lytic gene expression and productive infection, indicating the antiviral activity of PFAS in KSHV infection.

PFAS interacts with and deamidates RTA

PFAS is an enzyme, so we first determined whether the enzymatic activity is required for PFAS to inhibit RTA-dependent transcriptional activation using the enzyme (GAT)–deficient PFAS-ED mutant as we previously described (*9*). While PFAS wild type inhibited the RTA-mediated transcription of PAN and ORF57 promoters in a dose-dependent manner, the PFAS-ED mutant slightly increased the transcription of these promoters (fig. S3, A and B). We thus hypothesized that PFAS deamidates RTA to inhibit RTA-dependent transcriptional activation. To test this hypothesis, we probed the interaction between PFAS and RTA by coimmunoprecipitation. We found that endogenous PFAS co-precipitated with RTA in lysates of iSLK/rKSHV.219 cells in which KSHV lytic replication was induced (Fig. 2A). Moreover, an interaction between endogenous PFAS and exogenously expressed RTA was readily detected in transfected 293T cells, and KSHV infection further increased the levels of precipitated RTA and PFAS (Fig. 2B), likely due to increased RTA expression upon KSHV infection. These results indicate that RTA interacts with PFAS in transfected cells and in cells with KSHV lytic replication. Next, we depleted PFAS or overexpressed the PFAS-ED mutant and monitored RTA charge status by two-dimensional gel electrophoresis. Knockdown of PFAS and overexpression of the PFAS-ED mutant shifted RTA toward the negative pole (Fig. 2, C and D), indicating the reduced negative charge of RTA due to the inhibition of RTA deamidation. PFAS-ED expression had no effect on the charge status of β-actin (Fig. 2E). Collectively, these findings support the conclusion that endogenous PFAS promotes RTA deamidation in cells.

To identify the site(s) of deamidation, we purified RTA from transfected 293T cells without or with the expression of PFAS-ED and analyzed RTA by tandem mass spectrometry (MS) (fig. S3C). Comparative MS analysis identified two peptides containing deamidated residues of N37 and N225, which were specifically inhibited by the PFAS-ED mutant (Fig. 2F and fig. S3D). To validate the deamidation sites, we generated RTA containing N37D and N225D mutations, designated RTA-DD. PFAS-ED expression did not shift the deamidated RTA-DD mutant (fig. S3E), indicating that there are no other deamidation sites. Last, to test whether PFAS is sufficient to deamidate RTA, we purified glutathione *S*-transferase (GST)–RTA(N) from bacteria and PFAS or PFAS-ED from transfected 293T cells to high homogeneity (Fig. 2G) and performed an in vitro deamidation assay. Two-dimensional gel electrophoresis showed that PFAS, but not PFAS-ED, shifted RTA-N to the exact position of RTA-N-DD (Fig. 2H). Moreover, PFAS did not further shift RTA-N-DD. Together, these results indicate that PFAS is a bona fide deamidase of RTA.

Deamidation impairs RTA-mediated transcriptional activation

RTA-mediated transcriptional activation is necessary and sufficient for KSHV lytic replication. We used deamidated RTA mutants to determine how deamidation affects RTA-mediated transcription. Reporter assays showed that RTA-N37D (RTA-D37) and RTA-N225D (RTA-D225) were greatly impaired, and RTA-DD completely failed to activate the PAN promoter (Fig. 3A). A similar pattern of RTA-dependent transcription of the ORF57 promoter was observed for deamidated RTA mutants, albeit to a less extent (fig. S4A). These RTA deamidation mutants were expressed to levels comparable to RTA wild type (RTA-WT) in transfected 293T cells (fig. S4B). To investigate the effect of deamidation on KSHV lytic replication, we introduced D37 and D225 into the inducible bacterial artificial chromosome (iBAC) of KSHV in which the expression of RTA in the KSHV genome is driven by a doxycycline-inducible promoter (*22*). Unexpectedly, we repeatedly failed to obtain an SLK stable cell line that carries the KSHV iBAC with DD mutations in RTA, although SLK stable cells carrying KSHV iBAC with RTA-WT were readily obtained. Thus, we addressed this barrier with two alternatives. First, we established SLK stable cell lines that express RTA-WT or RTA-DD under the control of a doxycycline-inducible promoter. These stable cell lines were then infected with rKSHV.219. When RTA was induced with doxycycline, we examined the productive infection of KSHV by lytic gene and protein expression, DNA replication, and extracellular infectious virion. Although RTA-DD was expressed higher than RTA-WT with the same amount of doxycycline (fig. S4C), lytic replication of rKSHV.219 in SLK/RTA-DD cells was much lower than that in SLK/RTA-WT cells, as indicated by RFP expression (fig. S4D). RT-PCR analysis indicated that the expression

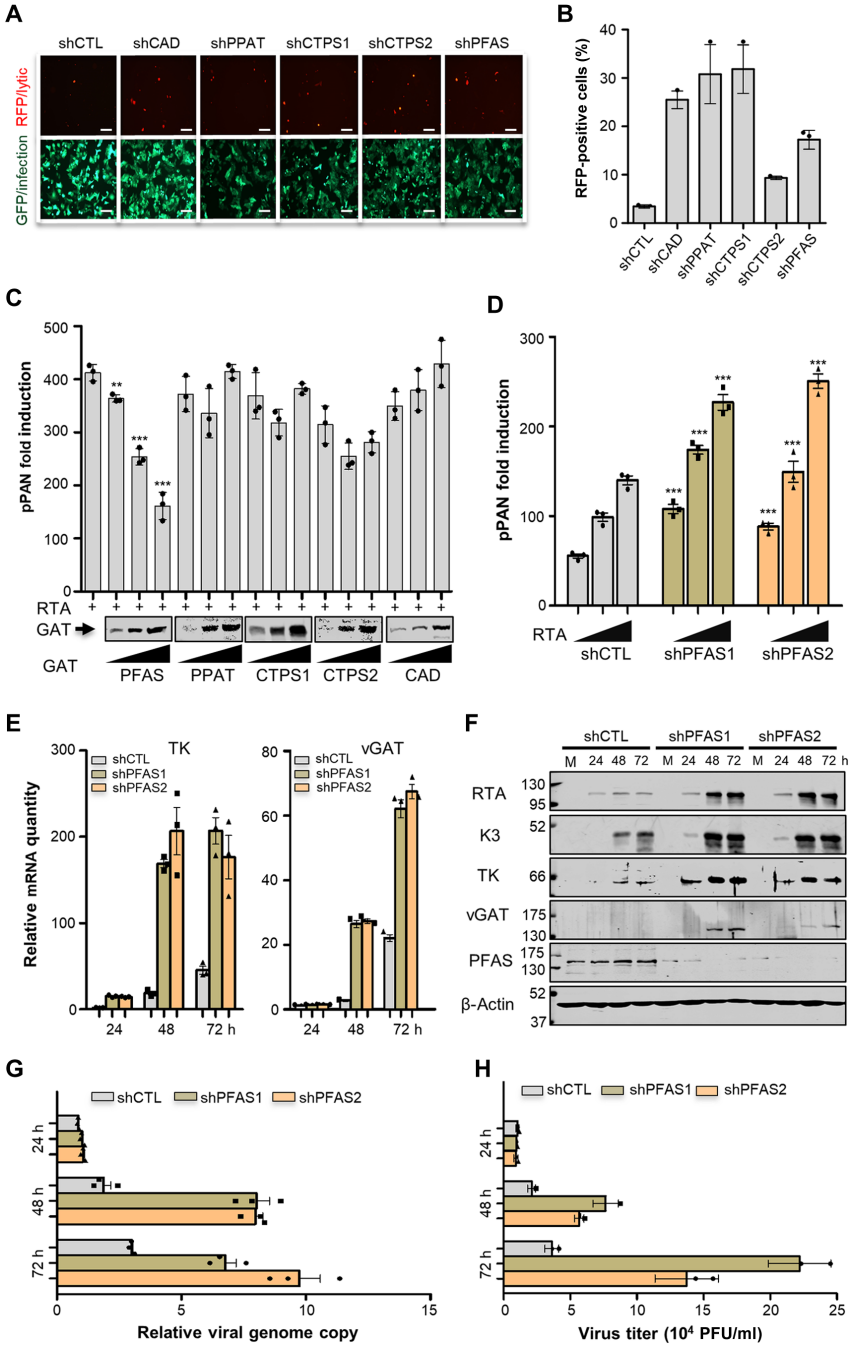

Fig. 1. Cellular PFAS negatively regulates RTA-dependent transcriptional activation. (**A**) 293T/RTA cells were infected with lentivirus carrying control (CTL) shRNA or shRNA targeting indicated GAT. At 48 hours after infection, cells were infected with rKSHV.219 and induced with doxycycline for RTA expression. Representative RFP$^+$ and GFP$^+$ cells of the screen were recorded at 24 hours after KSHV infection. Scale bars, 5 μm. (**B**) RFP$^+$ cells from (A) were quantified at 48 hours after infection by counting five randomly selected areas. The results are shown as the mean ± SD of three independent experiments in duplicate. $n = 3$. (**C**) 293T cells were transfected with plasmids containing RTA or the indicated GAT, and a reporter plasmid cocktail. RTA-mediated transcriptional activation of the PAN promoter was determined by luciferase activity at 30 hours after transfection. (**D**) 293T cells were infected with lentivirus carrying control shRNA (CTL) or shRNA against PFAS and selected with puromycin. Stable 293T cells were transfected with a plasmid containing RTA and a reporter plasmid cocktail. RTA-mediated transcriptional activation of the PAN promoter was determined by luciferase assay at 24 hours after transfection. For (C) and (D), the data are shown as the median ± SD of three independent experiments in duplicate ($n = 3$). $^{**}P < 0.01$ and $^{***}P < 0.001$, unpaired two-tailed Student's t test. (**E** to **H**) iSLK/rKSHV.219 cells were infected with lentivirus containing control (CTL) shRNA or shRNA against PFAS. Cells were induced with doxycycline (1.0 μg/ml) for the indicated times. When cells were harvested, total RNA was extracted for reverse transcription and RT-PCR analysis with primers specific for TK (or ORF21) and vGAT (or ORF75) (E), whole-cell lysates (WCLs) were analyzed by immunoblotting with antibodies against indicated viral and cellular proteins (F), viral genome copies were quantified by RT-PCR (G), and viral titer in the medium was determined by flow cytometry analysis of a KSHV-infected 293T monolayer (H). For (E) to (H), the data represent three independent experiments ($n = 3$). For (E), (G), and (H), the results are shown as the median ± SD of three independent experiments. PFU, plaque-forming units.

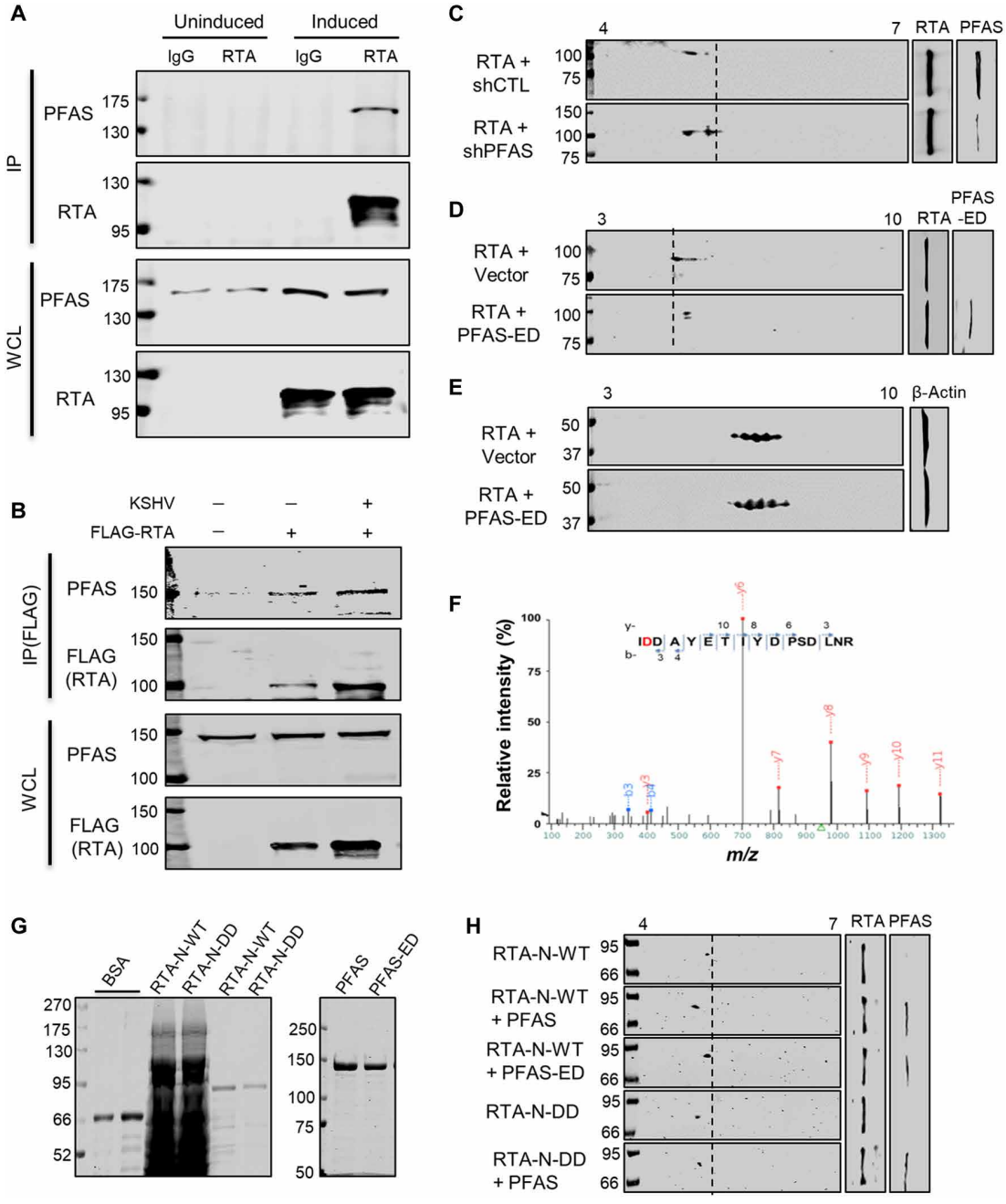

Fig. 2. PFAS deamidates RTA. (**A** and **B**) iSLK/rKSHV.219 cells were induced with doxycycline (1 μg/ml) and sodium butyrate (1 mM) for 48 hours (A). 293T cells were transfected with indicated plasmids for 24 hours and then either mock-infected or infected with KSHV (multiplicity of infection = 5) for 24 hours (B). WCLs were prepared, and immunoprecipitation was performed. Precipitated proteins and WCLs were analyzed by immunoblotting with indicated antibodies. (**C** to **E**) Stable 293T cells with control lentivirus (CTL) or lentivirus encoding shRNA against PFAS were transfected with a plasmid containing RTA (C). 293T cells were transfected with a plasmid containing RTA without or with a plasmid containing the PFAS-ED mutant. WCLs were prepared at 30 hours after transfection and analyzed by two-dimensional gel electrophoresis and immunoblotting with indicated antibodies (D and E). (**F**) RTA was purified from transfected 293T cells without or with PFAS-ED and analyzed by tandem MS. The mass/charge ratio (*m/z*) spectrum of the peptide containing D37 was shown with the deamidated D residue highlighted in red. (**G** and **H**) GST-RTA(N) and PFAS or PFAS-ED were purified from bacteria and 293T cells, respectively, and analyzed by silver staining (G). BSA, bovine serum albumin. In vitro deamidation was analyzed by two-dimensional gel electrophoresis and immunoblotting (H). All data present three independent experiments ($n = 3$).

of PAN, ORF57, and ORF59 in SLK/RTA-DD cells was one to two orders of magnitude lower than that in SLK/RTA-WT cells (fig. S4E). Moreover, viral genome copy number and extracellular infectious virion of SLK/RTA-DD cells were three- to fivefold lower than those of SLK/RTA-WT cells (fig. S4, F and G). These phenotypes of RTA-DD may have been underestimated, considering that RTA-WT expressed from the KSHV genome can compensate the loss of function of RTA-DD. Nevertheless, these results show that

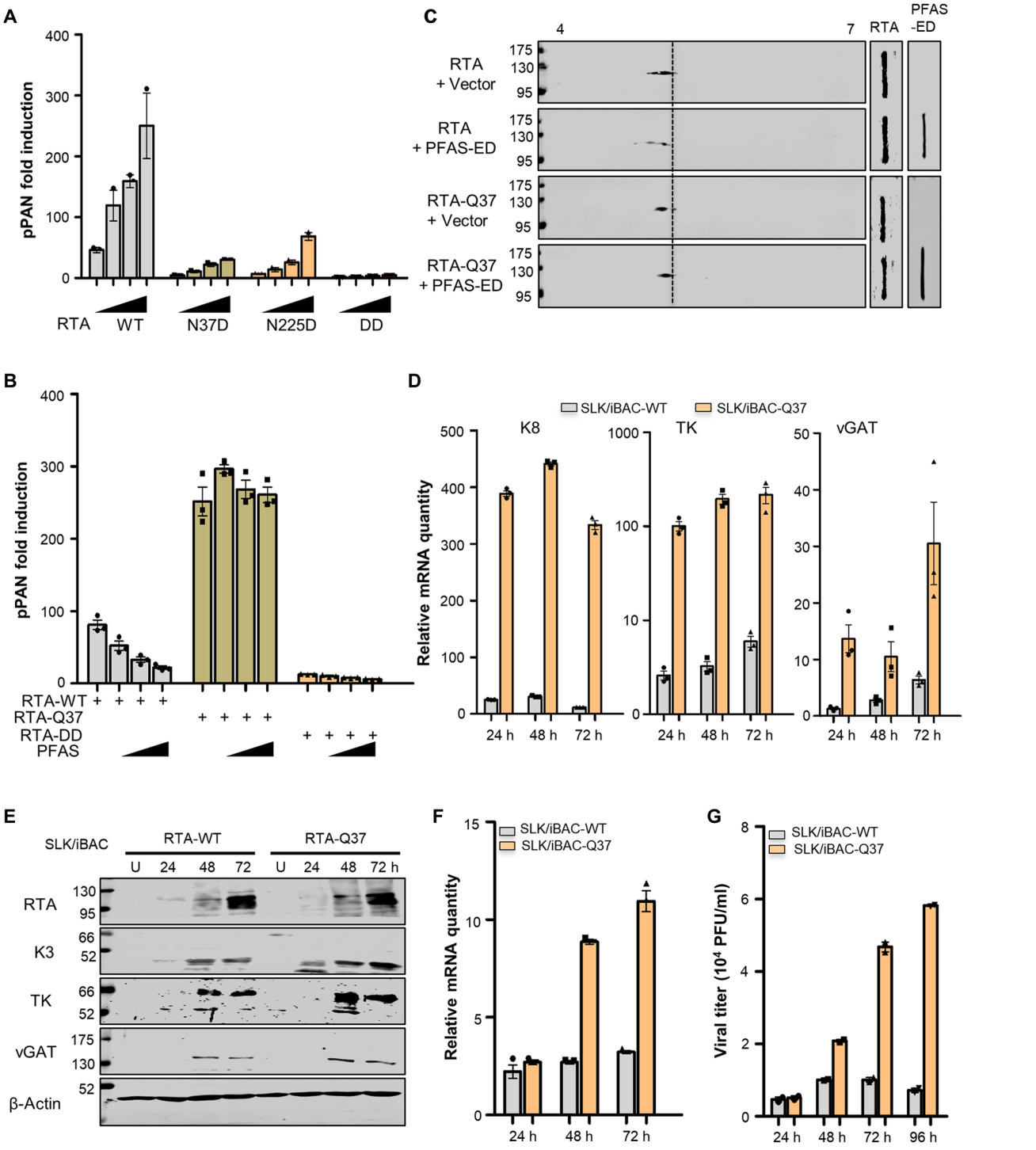

Fig. 3. Deamidation reduces RTA-mediated transcriptional activation. (**A**) 293T cells were transfected with a reporter plasmid cocktail and increasing amount of the plasmid containing RTA, RTA-D37, RTA-D225, or RTA-D37,225 (RTA-DD). RTA-dependent transcriptional activation of the PAN promoter was determined by luciferase assay at 30 hours after transfection. (**B**) 293T cells were transfected with a reporter plasmid cocktail; plasmids containing RTA-WT (WT), RTA-Q37 (Q37), or RTA-DD (DD); and increasing amount of a plasmid containing PFAS. RTA-dependent transcriptional activation of the PAN promoter was determined by luciferase assays. For (A) and (B), the results are shown as the median ± SD of three independent experiments with duplicate (n = 3). (**C**) 293T cells were transfected with plasmids containing indicated genes. WCLs were analyzed by two-dimensional gel electrophoresis and immunoblotting with antibodies against RTA or FLAG (PFAS-ED). The results represent three independent experiments (n = 3). (**D** to **G**) SLK/iBAC.RTA-WT or SLK/iBAC.RTA-Q37 cells were induced with doxycycline (1.0 μg/ml) for the indicated times. Cells were harvested and subjected to analyses by RT-PCR with primers specific for K8, TK, and vGAT (D); viral protein expression by immunoblotting (E); viral genome replication by RT-PCR (F); and viral titer in the medium by flow cytometry analysis of an infected 293T monolayer (G). For (D), (F), and (G), the results are shown as the median ± SD of three independent experiments (n = 3). For (E), the results represent three independent experiments (n = 3).

RTA-DD displays reduced transcriptional activation in KSHV lytic replication.

The second approach entails a gain-of-function mutant of RTA that is resistant to the PFAS-mediated deamidation. We have shown that N to Q mutations renders RIG-I resistant to UL37-mediated deamidation (*10*). We therefore tested whether N37Q (Q37) and N225Q (Q225) mutations in RTA resisted PFAS-mediated deamidation. Reporter assays indicated that RTA-Q37 was more potent than RTA-WT in activating the PAN promoter (fig. S5A). However, the RTA mutant containing both Q37 and Q225 was not as potent as RTA-WT, suggesting that the Q225 mutation negatively affects the transcriptional activation of RTA (fig. S5A). Furthermore, RTA-Q37, but not RTA-WT, was resistant to PFAS-mediated inhibition when RTA-dependent transcription was analyzed by reporter assays (Fig. 3B). Two-dimensional gel electrophoresis further confirmed that RTA-Q37 migrated farther toward the negative pole compared to RTA-WT and its migration was not shifted by the expression of PFAS-ED (Fig. 3C). Coimmunoprecipitation analysis indicated that RTA-Q37 demonstrated reduced interaction with PFAS compared to RTA-WT (fig. S5B), suggesting that N37 is crucial for PFAS-mediated deamidation of RTA. These results collectively show that RTA-Q37 is resistant to PFAS-mediated deamidation and inhibition, suggesting that N37 deamidation is required for N225 deamidation. If N37 deamidation is a prerequisite for N225 deamidation, this characteristic is reminiscent of the progressive phosphorylation of nuclear factor of activated T-cells (NFAT) primed by protein kinase A (PKA) (*23*). Nevertheless, we introduced the RTA-Q37 mutation into the KSHV iBAC genome. SLK cells carrying KSHV iBAC with RTA-WT or RTA-Q37 were established. Upon induction with doxycycline, the expression of KSHV lytic genes, including K8, TK, PAN, and vGAT, was ~10- to 20-fold higher in SLK/iBAC.RTA-Q37 cells than in SLK/iBAC.RTA-WT cells (Fig. 3D and fig. S5C). The elevated gene expression activated by RTA-Q37 was further supported by viral protein expression (Fig. 3E). Viral genome copy and extracellular infectious virion were increased by a factor of 3 to 6 at later time points, e.g., 36 to 96 hours after induction (Fig. 3, F and G). The increased lytic replication of iBAC.RTA-Q37, compared to that of iBAC.RTA-WT, was observed in HOK cells (fig. S5, D and E). Collectively, these results show that RTA-Q37 is resistant to PFAS-mediated deamidation and more potently induces KSHV lytic replication than RTA-WT does.

Deamidation impedes RTA nuclear localization

To understand how deamidation impairs RTA-mediated transcriptional activation, we modeled the RTA protein structure and found that N37 and N225 locate on the surface and flank a nuclear localization signal (NLS) (Fig. 4A). RTA primarily localizes in the nucleus through a bipartite NLS enriched with positively charged arginines and lysines. Conceivably, deamidation of N37 and N225 reduces the overall charge of the RTA NLS, thereby impeding the nuclear translocation of RTA. RTA-WT concentrated in the nucleus of iSLK stable cells, while RTA-DD was largely diffused in the cytoplasm (Fig. 4B). Semiquantitative analysis showed that RTA-WT was primarily nuclear in ~70% cells, while RTA-DD was detected in the nuclei of ~20% cells (Fig. 4C). Fractionation to separate the nuclei from the cytoplasm further demonstrated that ~20% of RTA-DD localized in the nucleus, compared to ~65% of RTA-WT in the nucleus (Fig. 4D). These results indicate that deamidation impairs RTA nuclear translocation, a process imperative for transcriptional activation.

To determine whether RTA deamidation controls its nuclear translocation during KSHV lytic replication, we probed RTA nuclear localization and deamidation in reactivated SLK cells after fractionation. Fractionation analysis indicated that RTA-WT was exclusively nuclear at 24 hours after induction, while it was primarily cytoplasmic at 72 hours after induction. In stark contrast, ~90% of RTA-Q37 demonstrated nuclear localization at 24 and 72 hours after induction (Fig. 4E). Immunofluorescence microscopy showed that the nuclear localization of RTA-WT at 24 hours after induction transitioned to primarily cytoplasmic at 72 hours after induction, while RTA-Q37 remained mostly nuclear at 24 and 72 hours after induction (Fig. 4F). We next examined RTA deamidation by two-dimensional gel electrophoresis. In SLK/iBAC.RTA-WT cells, RTA was shifted more toward the positive pole at 72 hours after induction than at 24 hours after induction (fig. S5F). However, RTA-Q37 traveled nearly the same distance at 24 and 72 hours after induction. We observed a species of RTA-Q37 that migrated to the position of the deamidated RTA-WT, which may be due to other posttranslational modifications such as phosphorylation or acetylation. Nevertheless, these data show that RTA deamidation regulates its nuclear translocation during KSHV lytic replication.

Deamidation impairs RTA interaction with importin

One of the best-defined mechanisms of protein nuclear import is mediated by the importin complex, which recognizes diverse NLSs and shuttles NLS-containing cargo molecules into the nucleus (*24*, *25*). The importin complex consists of heterodimeric α and β subunits. For a subset of cargo molecules, the β subunit can directly bind to the cargo and the α subunit is dispensable (*26*, *27*). Thus, we established stable cell lines that express distinct importin α and β subunits and probed the RTA and importin subunit interaction using coimmunoprecipitation. RTA was readily detected in protein complexes that were precipitated with importin β1 and β2, but not importin α1, α3, and α7 that represent three distinct clades (Fig. 5A) (*28*). Conversely, importin β1 and β2, but not α1, were precipitated with RTA (fig. S6A). To test whether importin α is dispensable for RTA interaction, we assessed a direct interaction between RTA and importin β1 using purified proteins. A GST pulldown assay showed that the GST–importin β1, but not GST alone, interacted with RTA in vitro, indicating that RTA directly interacts with importin β1 (Fig. 5B). Previous studies have identified the bimax2 peptide that effectively inhibited importin α–mediated nuclear translocation (*29*). We determined whether RTA is sensitive to the bimax2 peptide. As shown in Fig. 5C, the expression of an enhanced green fluorescent protein (EGFP)–bimax2 fusion had no apparent effect on the nuclear localization of RTA. This result is further supported by subcellular fractionation (fig. S6B). To determine the effect of protein deamidation on the interaction between RTA and importin β, we performed GST pulldown assay using RTA-WT and RTA-DD. This experiment demonstrated that deamidation severely impaired the RTA–importin β interaction (Fig. 5D). Moreover, RTA-WT, but not RTA-DD, was precipitated with importin β1 (Fig. 5E). The observation that RTA binds to both importin β1 and β2 subunit suggests that RTA can translocate into the nucleus via multiple pathways. We tested this hypothesis with the M9M peptide that was shown to inhibit the importin β2–mediated nuclear import (*30*). Both subcellular fractionation and fluorescence microscopy analysis demonstrated that the M9M peptide partly impeded RTA nuclear localization (fig. S6, C and D), supporting the role of importin β2 in RTA nuclear

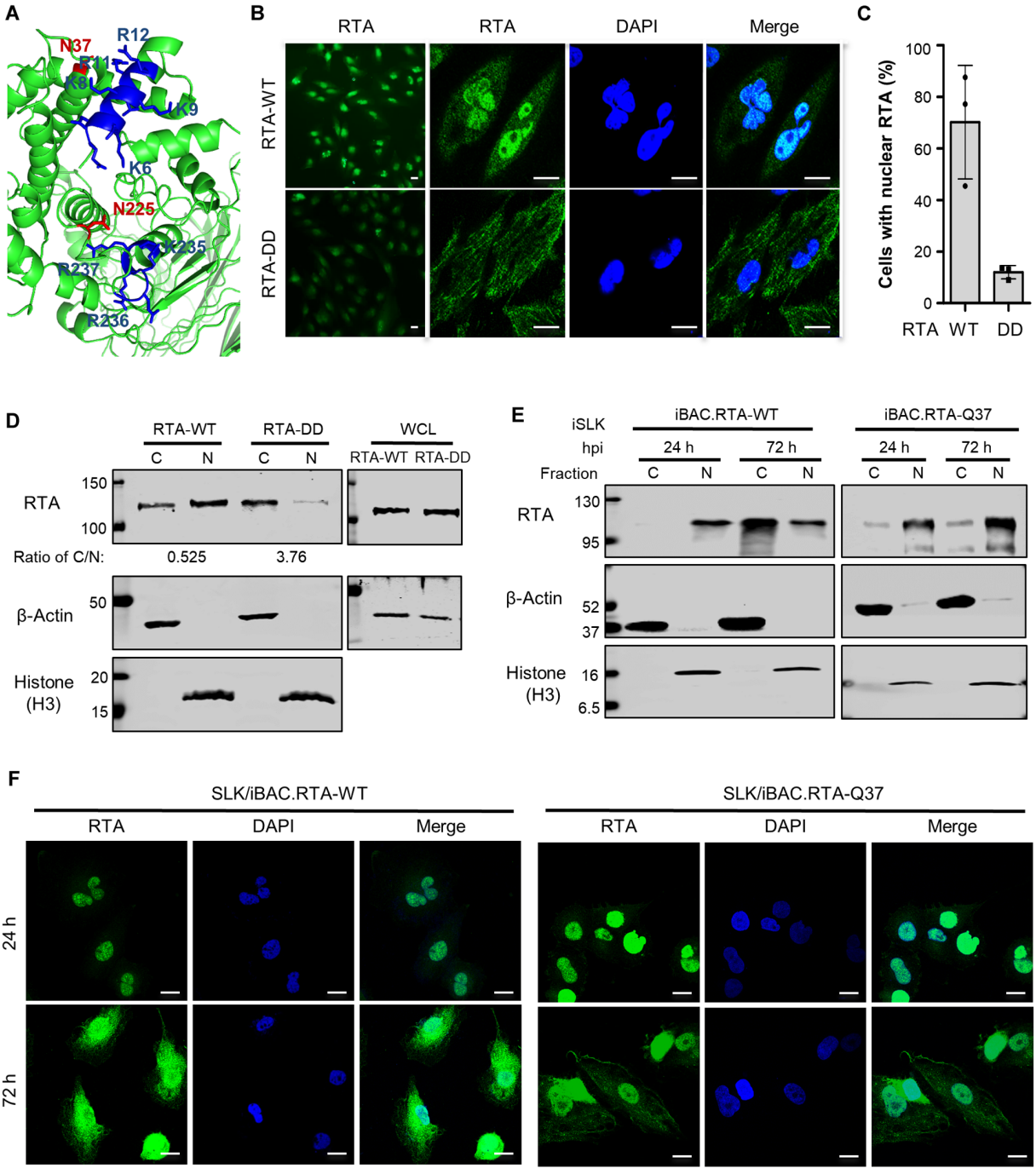

Fig. 4. Deamidation impedes RTA nuclear translocation. (**A**) A pdb file of RTA was modeled using the I-TASSER server from Zhang laboratory (see Methods for detail). Visualization of three-dimensional models of RTA was realized with PyMOL software. N37 and N225 (in green) locate on the surface and flank an NLS (in blue) that is enriched with arginine and lysine residues. (**B** and **C**) iSLK cells stably expressing RTA-WT or RTA-DD were analyzed by immunofluorescence microscopy. Representative images were shown. Scale bars, 5 μm (B). Cells with predominant nuclear RTA staining were counted (C). The results are shown as the median ± SD of three independent experiments ($n = 3$). (**D**) iSLK stable cell lines as described in (B) were harvested. WCLs were prepared and subjected to sequential centrifugation to obtain cytosolic (C) and nuclear (N) fractions. WCLs, cytosolic fractions, and nuclear fractions were analyzed by immunoblotting with indicated antibodies. (**E**) SLK/iBAC.RTA-WT (left) or SLK/iBAC.RTA-Q37 (right) cells were induced with doxycycline (1 μg/ml) and sodium butyrate (1 mM) for 24 or 72 hours. Cells were harvested at the indicated times and subjected to subcellular fractionation analysis by sequential centrifugation to obtain cytosolic (C) and nuclear (N) fractions that were analyzed by immunoblotting with indicated antibodies. (**F**) Lytic reactivated SLK/iBAC.RTA-WT or SLK/iBAC.RTA-Q37 cells were fixed at 24 or 72 hours after induction and analyzed by confocal microscopy. Representative images were shown. Scale bars, 20 μm. The results shown in (D) to (F) represent three independent experiments ($n = 3$).

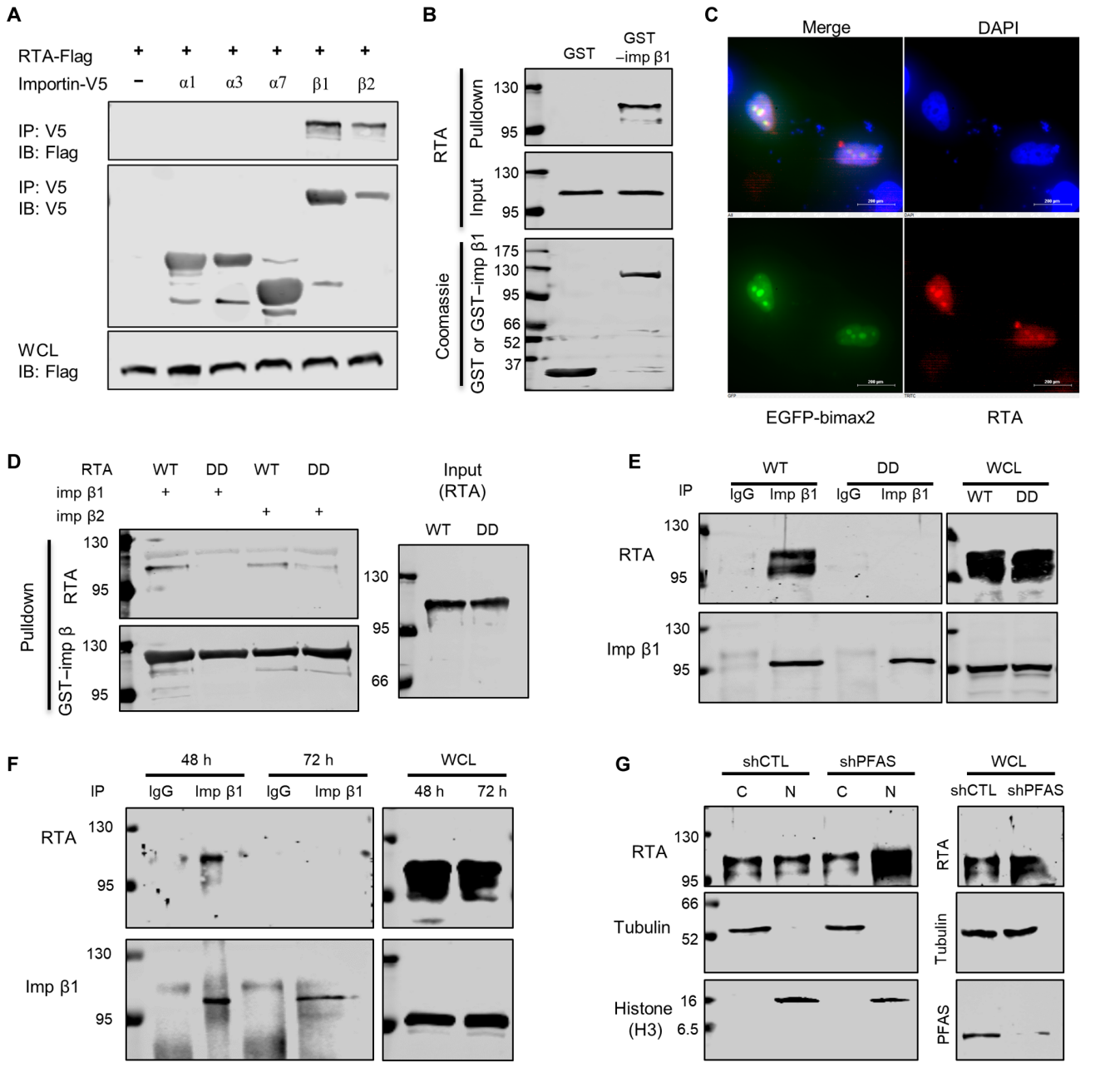

Fig. 5. Deamidation impairs RTA binding to importin. (**A**) 293T cells were transfected with plasmids containing FLAG-tagged RTA-WT and the indicated V5-tagged importins. WCLs were incubated with anti-V5 antibody. The precipitated proteins and WCLs were analyzed by immunoblotting with indicated antibodies. (**B**) Glutathione agarose loaded with GST or recombinant GST–importin β1 was incubated with purified RTA. Precipitated proteins and RTA (input) were analyzed by immunoblotting with anti-RTA antibody, while GST and GST–importin β1 were analyzed by Coomassie staining (bottom). (**C**) SLK/iBAC.RTA-WT cells were induced with doxycycline (1 μg/ml) for 24 hours and then transfected with a plasmid containing EGFP-bimax2 for 24 hours. Cells were analyzed by immunofluorescence staining and microscopy. (**D**) Glutathione agarose loaded with GST fusions containing either importin β1 (imp-β1) or β2 (imp-β2) was incubated with WCLs containing RTA-WT (WT) or RTA-DD (DD). Precipitated proteins and WCLs (Input) were analyzed by immunoblotting with anti-RTA antibody (right). GST–importin β1 and GST–importin β2 were analyzed by Coomassie staining. (**E**) 293T cells were transfected with plasmids containing RTA-WT (WT) or RTA-DD (DD) mutant. WCLs were prepared and precipitated with control immunoglobulin G (IgG) or antibody against importin β1 (Imp-β1). Precipitated proteins and WCLs were analyzed by immunoblotting with indicated antibodies. (**F**) iSLK/rKSHV.219 cells were induced with doxycycline (0.5 μg/ml) and sodium butyrate (1 mM) for the indicated times. Immunoprecipitation and immunoblotting were performed as described in (E). (**G**) iSLK/rKSHV.219 cells were transduced with control lentivirus (CTL) or lentivirus encoding shRNA against PFAS, followed by doxycycline and sodium butyrate induction for 72 hours. Cells were harvested for cellular fractionation to obtain cytosolic (C) and nuclear (N) fractions that, along with WCLs, were analyzed by immunoblotting with indicated antibodies. The results shown in (A), (B), and (D) to (G) represent three independent experiments ($n = 3$).

translocation. Consistent with RTA deamidation during late stages of KSHV lytic replication, RTA was precipitated with importin β1 at 48 hours after induction but was not precipitated at 72 hours after induction (Fig. 5F). Depletion of PFAS increased RTA nuclear accumulation during KSHV lytic replication (Fig. 5G). These results demonstrate that RTA is delivered to the nucleus by importin β subunits and deamidation impairs RTA binding to importin β, thereby impeding RTA nuclear translocation.

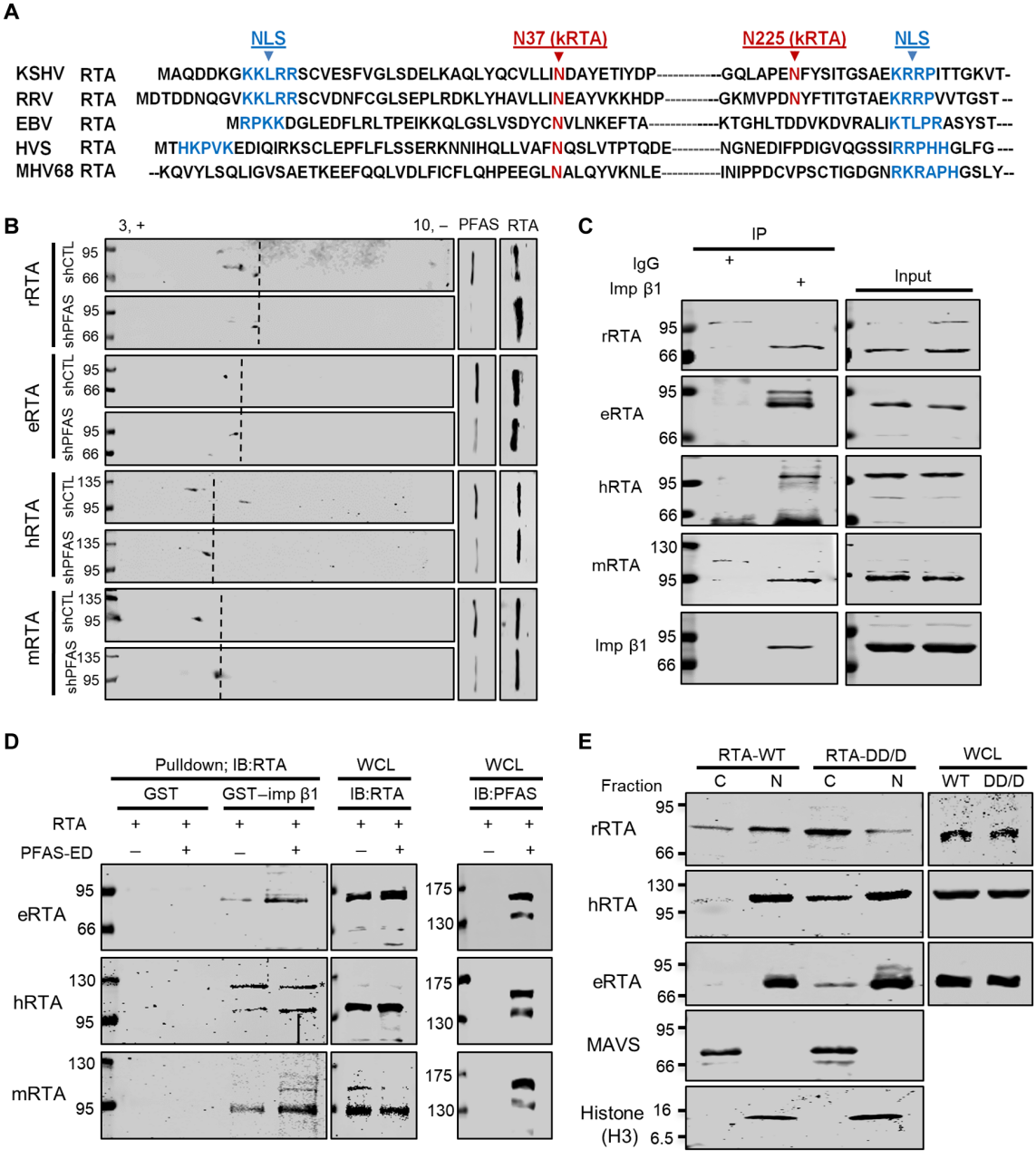

Fig. 6. PFAS-mediated deamidation regulates the nuclear import of RTA proteins of gamma herpesviruses. (**A**) Alignment of RTA proteins of KSHV, RRV, EBV, HVS, and MHV68 shows the bipartite NLS and the two deamidation sites corresponding to N37 and N225 of KSHV RTA. (**B**) 293T stable cells carrying control shRNA or PFAS shRNA were transfected with a plasmid containing RRV RTA (rRTA), EBV RTA (eRTA), HVS RTA (hRTA), or MHV68 RTA (mRTA). WCLs were prepared at 30 hours after transfection and analyzed by two-dimensional gel electrophoresis and immunoblotted for RTA (left). WCLs were analyzed by immunoblotting with antibodies against PFAS and RTA (right). (**C**) 293T cells transfected with plasmids containing rRTA, eRTA, hRTA, or mRTA. WCLs were precipitated with a control IgG or antibody against importin β1. Precipitated proteins and WCLs were analyzed by immunoblotting with indicated antibodies. (**D**) Glutathione agarose loaded with GST or GST–importin β1 (GST–imp β1) were incubated with WCLs prepared from 293T cells transfected with a plasmid containing eRTA, hRTA, or mRTA, without or with a plasmid containing PFAS-ED. Precipitated proteins and WCLs were analyzed by immunoblotting with indicated antibodies. (**E**) 293T cells were transfected with wild type (WT) or the deamidated mutant (DD/D) of rRTA, hRTA, or eRTA. Sites of N>D mutations were highlighted in (A). Nuclear (N) and cytosolic (C) fractions were obtained by sequential centrifugation and analyzed by immunoblotting with indicated antibodies. WCLs were analyzed for the expression of RTA wild type and the DD/D mutant (right panels). The results shown in (B) to (E) represent three independent experiments ($n = 3$).

PFAS-mediated deamidation regulates the nuclear import of gamma herpesvirus RTA proteins

RTA is shared among gamma herpesviruses, including human EBV and KSHV, nonhuman primate rhesus rhadinovirus (RRV) and herpesvirus saimiri (HVS), and murine gamma herpesvirus 68 (MHV68) (*17*, *31*–*33*). We postulated that all RTA proteins are targeted by cellular PFAS and protein deamidation. Sequence alignment revealed that RRV RTA (rRTA) contained N residues at positions equivalent to N37 and N225 of KSHV RTA (kRTA), while RTA proteins of EBV (eRTA), HVS (hRTA), and MHV68 (mRTA) only had a single N residue corresponding to N37 of kRTA (Fig. 6A). Furthermore, a bipartite NLS was identified in rRTA, eRTA, and hRTA, whereas mRTA contained an NLS equivalent to that of kRTA proximal to the N225 site (Fig. 6A). We first determined whether PFAS knockdown and PFAS-ED overexpression inhibited the deamidation of these RTA proteins. Two-dimensional gel electrophoresis indicated that PFAS depletion shifted all RTA proteins toward the negative pole (Fig. 6B), indicative of inhibition of the PFAS-mediated deamidation. Among these RTA proteins, rRTA had the most significant shift, while eRTA had the least shift upon PFAS depletion. A similar effect of PFAS-ED on the charge status of all RTA proteins was observed (fig. S7A). To exclude a nonspecific effect, we examined the effect of the GAT-deficient mutant of CAD (CAD-C/S) on RTA charge status. The CAD-C/S mutant did not alter the charge of kRTA, eRTA, and mRTA, while it slightly shifted rRTA toward the negative pole (fig. S7B), supporting the specificity of PFAS-mediated deamidation of RTA proteins. To test whether gamma herpesvirus RTA proteins are cargoes of the importin complex, we precipitated importin β1 from lysates of 293T cells expressing gamma herpesvirus RTAs and found that all RTA proteins were readily detected in protein complexes precipitated by importin β1 (Fig. 6C). Furthermore, PFAS-ED overexpression increased the interaction of importin β1 with eRTA, hRTA, and mRTA (Fig. 6D). Thus, PFAS-ED inhibits deamidation and promotes the importin binding of RTA proteins. To assess the effect of deamidation on RTA nuclear translocation, we generated deamidated mutants of rRTA (N39, 227D; DD), hRTA (N39D), and eRTA (N31D) and probed the nuclear and cytosolic fractions of these RTA mutants. These deamidated RTA mutants demonstrated increased cytosolic localization compared to their wild-type counterparts, with deamidated rRTA being the most prominently increased (Fig. 6E). These results collectively show that RTA interacts with importin β via a positively charged NLS. Deamidation of residues flanking this NLS sequence impairs RTA interaction with importin β, thereby reducing its nuclear translocation and transcriptional activation (fig. S7C). Taken together, PFAS-mediated deamidation appears to control the nuclear import of all gamma herpesvirus RTA proteins and is a general mechanism governing the nuclear import of RTA proteins.

DISCUSSION

In this study, we identified five nucleotide-synthesizing enzymes that restrict the lytic replication of KSHV. As obligate intracellular pathogens, viruses rely on cellular metabolic enzymes to propagate and nucleotide-synthesizing enzymes are crucial for viral productive infection. Genomes of herpesviruses encode multiple enzymes participating in nucleotide metabolism, which presumably circumvents the limited catalytic activity of host enzymes during productive viral infection. Furthermore, recent studies demonstrated that cellular metabolic pathways, such as glycolysis, lipid, and nucleotide synthesis, were activated and funneled to favor viral replication (*34*–*36*). Thus, the antiviral activity of these nucleotide-synthesizing enzymes is seemingly counterintuitive to this prevailing notion. The antiviral activity of cellular metabolic enzyme, however, is not unprecedented. SAMHD1, a cellular deoxyribonucleotide triphosphates (dNTP) phosphohydrolase, reduces the nucleotide pool to block HIV replication in immune cells such as monocytes and dendritic cells. If these cellular metabolic enzymes are essential for viral replication, the antiviral activity of these cellular GATs thus installs an obstacle that is difficult for viruses to overcome. Direct inhibition of these metabolic enzymes will halt cell proliferation and viral replication. Perhaps, the best scenario is that viruses redirect cellular GATs to modulate cellular and viral targets, which will facilitate viral infection. Our previous report that vGAT pseudoenzymes recruit PFAS to deamidate RIG-I and inactivate antiviral cytokine production supports this possibility (*9*).

Mechanistically, PFAS, a purine-synthesizing enzyme, deamidates the master transcription factor RTA to dampen viral lytic gene expression. Our study shows that RTA contains a bipartite NLS that can use both importin β1 and β2, but not α subunits, for its nuclear entry. This bipartite NLS of RTA is distinct from those of the classical and PY type (*24*, *37*, *38*). Deamidation of asparagine residues that flank the positively charged NLS of RTA impaired its interaction with importin β subunits, thus impeding RTA nuclear translocation. As such, the deamidation-resistant RTA-Q37 more potently activated lytic gene expression and productive infection of KSHV, while the deamidated RTA was highly impaired to trans-activate KSHV lytic gene expression. The result that RTA-Q37 is resistant to PFAS-mediated deamidation is interesting and suggests that the deamidation of N37 is required for that of N225. SLK cells carrying the KSHV genome containing the deamidated RTA failed to propagate, supporting the critical regulatory role of RTA deamidation. The nuclear import of RTA modulated by deamidation is similar to that of known importin cargoes, such as fused in sarcoma (FUS) (*39*) and the nuclear poly(A) binding protein 1 (PABPN1) (*40*), whose nuclear import is fine-tuned by arginine methylation (*41*). A feature shared by deamidation and arginine methylation is the reduction in the charge of the NLS of importin substrates, implying their overlapping roles in this fundamental process. Alternatively, PFAS-mediated RTA deamidation and inhibition of viral transcriptional activation may facilitate latent infection of herpesviruses by repressing RTA-dependent lytic gene expression. Persistence-prone herpesviruses may exploit this host regulatory mechanism to perpetuate its persistency (*42*, *43*), thus coupling viral infection to the cellular metabolic status.

RTA proteins constitute a group of transcription factors important for the infection of gamma herpesviruses (*17*). PFAS may therefore exert antiviral activity against these herpesviruses by deamidating and inhibiting RTA-mediated transcriptional activation. In addition to deamidation, RTA was reported to be subject to regulation by a diverse panel of posttranslational modifications and cellular factors (*44*–*49*). Although this study demonstrates that PFAS deamidates RTA to restrict KSHV lytic replication, deamidation of other viral and cellular proteins may contribute to the antiviral activity of PFAS. Considering that nucleic acid anabolic enzymes are crucial for cellular and viral macromolecular synthesis, the antiviral activity of these GATs against gamma herpesviruses is unexpected. In mammalian cells, the de novo synthetic pathways are activated to

replenish the nucleotide pool when it is low. The rate-limiting enzymes of de novo purine and pyrimidine synthesis are directly inhibited by their final products of either pathway, providing a negative feedback mechanism to achieve homeostasis (*50*). Thus, highly active nucleotide-synthesizing GATs would reflect the low level of nucleotide pool and therefore biological processes consuming nucleotides have to be curtailed to conserve nucleotides until the nucleotide pool is restored. Transcription, among other biological processes, is a main nucleotide-consuming activity and a prerequisite for other nucleotide-consuming processes such as DNA replication and ribosome biogenesis. We therefore propose that protein deamidation conveyed by the cellular nucleotide-synthesizing GATs targets transcription to reduce nucleotide consumption when the cellular nucleotide pool is low. Inhibition of viral transcription is likely a part of the cellular metabolic regulation in virus-infected cells. Reducing transcription and subsequent key steps underlying KSHV lytic replication is predicted to balance the nucleotide consumption with its supply. These activities may coordinate viral replication processes, which ultimately tailor the viral lytic replication according to cellular metabolic supplies. In doing so, viral productive infection is tempered to engender minimal stress and perturbation on cellular homeostasis, which is particularly important for persistent viruses such as herpesviruses. Further investigation is necessary to test this hypothesis. In addition, we previously reported that MHV68 hijacked PFAS to evade antiviral cytokine production (*9*). The phenotype of PFAS in gamma herpesvirus infection is the sum of multiple opposing activities, and therefore, each activity is likely underestimated. This "neutralized" phenotype presumably reflects the millions of years of coevolution between herpesviruses and their natural hosts. Whether protein deamidation operates to control nuclear import of cellular proteins (e.g., transcription factors) remains an open question. Nevertheless, these data uncover a crucial role of deamidation in regulating protein nuclear import, expanding the known functional repertoire of protein deamidation.

METHODS

Cell lines, antibodies, and reagents

HEK293T (human kidney epithelial cell origin) and SLK were cultured in Dulbecco's modified Eagle's medium (Corning) supplemented with 10% heat-inactivated fetal bovine serum (HyClone), penicillin (100 U/ml), and streptomycin (100 μg/ml). The SLK cell line was previously identified as epithelial cell, rather than endothelial cell. This cell line, containing the recombinant rKSHV.219, provides a useful system to examine KSHV lytic replication and to produce high titer of KSHV virus. HOK cells were provided by R. Sun (University of California, Los Angeles) and cultured with keratinocyte growth medium (Lonza). All cell lines were confirmed being free of mycoplasma infection and were periodically checked for mycoplasma contamination.

Escherichia coli GS1783 carrying iBAC of the KSHV genome was provided by F. Zhu (Florida State University). RTA(N) construct was described previously (*51*) and provided by K. Lan (Wuhan University). PFAS enzyme (GAT)–deficient mutant PFAS-ED and luciferase reporter plasmids for the PAN and K57 promoter were prepared as previously described (*9*). Antibodies against GST (Z-5), GFAT1 (H49), GFAT2 (H300), and GFP (FL) were purchased from Santa Cruz Biotechnology. Antibodies against V5 (ab177487), PFAS (ab82755), CAD (ab97340), and β-actin (ab8226) were purchased from Abcam. Antibodies against FLAG (M2, Sigma), importin α1 (sc-101292, Santa Cruz Biotechnology), importin β1 (NB100-94993, Novus Biologicals), importin β2 (sc-32314, Santa Cruz Biotechnology), human influenza hemagglutinin (HA) (MMS-101P, BioLegend), goat anti-rabbit/mouse immunoglobulin G (H+L) Alexa Fluor 488 (A-11034 and A32723, Invitrogen), tubulin (DM1A, Cell Signaling), and histone H3 (1B1B2, Cell Signaling) were purchased from the indicated suppliers. Human MAVS, KSHV RTA (ORF50), ORF75 (vGAT), and ORF21 (kTK) polyclonal antibodies were generated from Cocalico Biologicals (Reamstown, PA) using standard procedures. Polyclonal antibodies were purified by affinity chromatography using antigens immobilized on polyvinylidene difluoride membrane or peptides conjugated to CarboxyLink Coupling Resin and EDC (Thermo Fisher Scientific). Rabbit polyclonal anti-K3 antibody was generated as previously described (*52*). Lipofectamine 3000 was purchased from Life Technologies. Hypoxanthine, CTP, uridine, NAD, and ivermectin were purchased from Sigma. The control shRNA and shRNAs against human GATs, including GFAT1, GFAT2, PFAS, ASNSD, CAD, NADSYN1, CTPS1, CTPS2, GFPT1, GFPT2, GMPS, PPAT, and ASNS, were purchased from Thermo Fisher Scientific and Sigma.

Site-directed mutagenesis and DNA transfection

Codons corresponding to asparagine residues of RTAs were mutated to aspartate (D) or glutamine (Q) using the QuikChange Site-Directed Mutagenesis Kit (Stratagene) and confirmed by sequencing. For transfection with 293T cells, calcium phosphate or polyethylenimine was used when cells were of ~50 to 60% confluency. For BAC DNA transfection in SLK cells, Lipofectamine 3000 was used according to the manufacturer's instructions. Cells in each well of a 24-well plate were transfected with approximately 1 μg of BAC DNA, and SLK/iBAC-positive cells were selected with hygromycin B (200 μg/ml) at 48 hours after transfection.

Key plasmid construction

The importin plasmids were either obtained directly from the human complementary DNA (cDNA) library as in pLX307 vector or cloned into pCDH vector with a C-terminal V5 tag. BIMAX2 (RRRRRRKRKREWDDDDDPPKKRRRLD) (*29*) and M9M (GGSYNDFGNYNNQSSNFGPMKGGNFGGRFEPYANPTKR) (*30*) were cloned into pEGFP-C2 vector to enable the expression of N-terminal EGFP fusion proteins. RTA-RFP was prepared by cloning of RTA into a modified pcDNA3 vector containing a C-terminal RFP sequence.

Luciferase reporter assay

293T cells seeded in 24-well plates were transfected with the PAN or ORF57 promoter reporter cocktail (100 ng total), with plasmids containing RTA-WT or mutants. Cell lysates were prepared at 30 hours after transfection using lysis buffer (Promega). Luciferase activity was determined by a microplate reader (FLUOstar Omega) using centrifuged whole-cell lysates (WCLs). β-Galactosidase was used as an internal control.

Lentivirus-mediated stable cell line construction

iSLK/RTA-WT and iSLK/RTA-DD stable cell lines were established using Tet-On 3G Tetracycline Inducible Gene Expression Systems. Briefly, 293T cells were transfected with the packaging plasmids VSV-G, Gag-pro, Vpr-pol, Tet-off, and tat-IRES-rev and the

TetONE-RTA-WT or TetONE-RTA-DD lentiviral expression vector. For making shRNA lentivirus, 293T cells were cotransfected with packaging plasmids VSV-G, DR8.9, and the shRNA lentiviral plasmid as previously described (*53*). At 48 hours after transfection, the supernatant was harvested and filtered, and viruses were concentrated by ultracentrifugation. SLK or 293T cells were spin-infected (1800 rpm) with lentivirus in the presence of polybrene (8 μg/ml) for 45 min. Cells were selected with puromycin (1 μg/ml) at 48 hours after infection.

Protein expression and purification

293T cells were transfected with an expression vector containing the FLAG-tagged protein of interest. Cells were harvested and lysed with Triton X-100 buffer [25 mM Hepes (pH7.5), 100 mM NaCl, 10% glycerol, 1 mM EDTA, and 1% Triton X-100] supplemented with protease inhibitor cocktail (Roche). WCLs were sonicated and centrifuged at 12,000 rpm for 30 min. Supernatant was filtered, precleared with protein A/G agarose beads at 4°C for 1 hour, and then incubated with anti-FLAG M2 agarose beads at 4°C for 4 hours. Agarose beads were washed extensively with lysis buffer and eluted with 3×FLAG peptide (0.2 mg/ml). Eluted proteins were analyzed by SDS—polyacrylamide gel electrophoresis (PAGE) and Coomassie/silver staining.

For recombinant GST-RTA(N) and GST–importin β purification, *E. coli* BL21 (DE3) was induced with 0.1 mM isopropyl-β-D-thiogalactopyranoside at 20°C overnight. Cell pellets were harvested and lysed. After sonication and centrifugation, cell lysates were incubated with glutathione Sepharose 4B beads (GE Healthcare) for 4 hours at 4°C. Sepharose beads were washed extensively with lysis buffer, and GST-RTA(N) was eluted with 10 mM reduced glutathione. Purified GST, GST-RTA(N), and GST–importin β were analyzed by SDS-PAGE and Coomassie staining.

Coimmunoprecipitation, GST pulldown, and immunoblotting

Transfected 293T cells or reactivated iSLK/rKSHV.219 cells [sodium butyrate (1 mM) and doxycycline (1 μg/ml)] were harvested and lysed with NP-40 buffer [50 mM tris-HCl (pH8.0), 150 mM NaCl, and 1% NP-40] supplemented with protease inhibitor cocktail (Roche). WCLs were sonicated, centrifuged, and precleared with protein A/G agarose for 1 hour. Precleared cell lysates were then incubated with anti-FLAG M2 agarose beads (Sigma-Aldrich) for 4 hours at 4°C or anti–importin β1/anti-kRTA antibodies overnight following protein A/G agarose incubation for 1 hour at 4°C. The agarose beads were washed extensively, and protein was eluted with 1× SDS-loading buffer by boiling for 10 min. Samples were then subjected to SDS-PAGE and immunoblotting.

For GST pulldown with importin β, 293T cells were transfected with plasmids containing RTA-WT or RTA-DD and then lysed in binding buffer [20 mM tris-HCl (pH 7.5), 100 mM NaCl, 10% glycerol, and 0.5% NP-40] plus protease inhibitor cocktail (Roche). Cell lysates were centrifuged and then precleared with glutathione beads. Precleared cell lysates were incubated with glutathione resin loaded with GST or GST–importin β (~4 μg of protein). After incubation at 4°C for 4 to 6 hours, the resin was washed three times in binding buffer and then proteins were eluted, resolved by SDS-PAGE, and analyzed by immunoblotting. All immunoblotting analyses were performed using the indicated primary antibodies (1:1000 dilution) and IRDye800-conjugated secondary antibodies (1:10,000 dilution) (LI-COR). Proteins were visualized using an Odyssey infrared imaging system (LI-COR).

Subcellular fractionation

Cells (2×10^6) were washed with cold phosphate-buffered saline (PBS) and resuspended in 150 μl of hypotonic buffer [20 mM tris-HCl (pH7.4), 10 mM NaCl, and 3 mM $MgCl_2$] supplemented with protease inhibitor cocktail for 15 min on ice. NP-40 detergent (0.5%) was then added, and the sample was vortexed for 10 s, followed by centrifugation for 10 min at 3000 rpm at 4°C. The supernatant was collected as the cytoplasmic fraction. The nuclear pellet was washed and resuspended in 150 μl of complete cell extraction buffer [10 mM tris (pH 7.4), 2 mM Na_3VO_4, 100 mM NaCl, 1% Triton X-100, 1 mM EDTA, 10% glycerol, 1 mM EGTA, 0.1% SDS, 1 mM NaF, 0.5% deoxycholate, and 20 mM $Na_4P_2O_7$] supplemented with protease inhibitor cocktail for 30 min on ice with vortexing at 10-min intervals. After centrifugation, the supernatant was collected at 18,000*g* for 30 min as the nuclear fraction. Proteins were normalized by Bradford protein assay and analyzed by SDS-PAGE and immunoblotting with indicated antibodies.

Immunofluorescence microscopy

iSLK/RTA-WT, iSLK/RTA-DD, SLK/iBAC.RTA-WT, or SLK/iBAC.RTA-Q37 cells were processed as previously described (*53*). Briefly, cells were fixed with 4% paraformaldehyde and permeabilized with 1% Triton X-100 buffer. After being blocked with goat serum, cells were incubated with primary mouse monoclonal anti-FLAG M2 antibody or polyclonal anti-RTA (1:100 dilution) serum. Cells were then incubated with Alexa Fluor 488–congugated goat secondary antibody (1:500 dilution), stained with 4′,6-diamidino-2-phenylindole (DAPI), and analyzed with confocal microscope (Nikon). Cells expressing fluorescent fusion proteins were fixed with 4% paraformaldehyde and directly analyzed by immunofluorescence microscope (Nikon). Representative images were shown for all analyses.

Virus preparation and infection

iSLK/rKSHV.219, SLK/iBAC.RTA-WT, and SLK/iBAC.RTA-Q37 cells were reactivated with doxycycline (1 μg/ml) without or with 1 mM sodium butyrate for up to 96 hours as previously described (*22*). iSLK/RTA-WT or iSLK/RTA-DD cells infected with rKSHV.219 were induced with doxycycline (1 μg/ml) up to 96 hours. The supernatant containing infectious virion particles was collected and centrifuged at 1000*g* for 10 min. Virus was concentrated by ultracentrifugation at 32,500*g* for 2 hours, if necessary. Virus titer was quantified on 293T monolayers by flow cytometry with FACSCalibur (BD Biosciences, San Jose, CA). Data collected from fluorescence-activated cell sorting were analyzed with FlowJo software (TreeStar). Viral genomic DNA was purified from infected cells with the DNeasy Blood and Tissue Kit (Qiagen) for KSHV genome replication by quantitative RT-PCR (qRT-PCR)

Quantitative RT-PCR

qRT-PCR was performed as previously described (*10*). 293T, SLK, or HOK cells were harvested at various time points for total RNA extraction using TRIzol reagent (Invitrogen). cDNA was synthesized using a PrimeScript RT kit according to the manufacturer's instruction (Invitrogen). cDNA was diluted 20-fold, and qRT-PCR was performed using SYBR Green Master Mix (Applied Biosystems) on the Applied Biosystems StepOnePlus Real-Time PCR System. Relative mRNA expression for each target gene was calculated by the $2^{-\Delta\Delta Ct}$ method using β-actin as an internal control. Sequences of qRT-PCR primers are shown in Table 1.

Two-dimensional gel electrophoresis

Two-dimensional gel electrophoresis was performed as previously reported with minor modifications (*9*, *10*). Briefly, protein from cells (1×10^6) was isolated using TRIzol reagent (Invitrogen) and dissolved in 150 μl of rehydration buffer [8 M urea, 2% CHAPS, 50 mM dithiothreitol (DTT), 0.5% immobilized pH gradient (IPG) buffer, and 0.002% bromophenol blue]. After centrifugation at 20,000*g* for 30 min, the supernatant was loaded on Immobiline DryStrips (GE Healthcare) for isoelectric focusing (IEF) with a program comprising 20 V, 12 hours (rehydration); 300 V, 1 hour; 1000 V, 1 hour; 2000 V, 1 hour; 5000 V, 3 hours; and 5000 V, 4 hours. After IEF, strips were incubated with SDS equilibration buffer [50 mM tris-HCl (pH 8.8), 8 M urea, 30% glycerol, 2% SDS, and 0.001% bromophenol blue] containing 70 mM DTT for 15 min and then SDS equilibration buffer containing 2-iodoacetamide (25 μg/ml) for 15 min. Strips were washed with SDS-PAGE buffer, resolved by SDS-PAGE, and analyzed by immunoblotting.

In vitro deamidation assay

GST-RTA(N)-WT or GST-RTA(N)-DD was expressed and purified from *E. coli* strain BL21. FLAG-tagged PFAS or PFAS-ED was purified from transfected 293T cells. In vitro on-column deamidation of RTA(N) was performed as previously reported (*9*, *10*). Briefly, 1 μg of PFAS/PFAS-ED and 0.5 μg of GST-RTA(N) (immobilized on glutathione-conjugated agarose) were added to a total volume of 50 μl. The reaction was carried out at 37°C for 45 min in deamidation buffer [50 mM tris-HCl (pH 7.5), 100 mM NaCl, and 5 mM $MgCl_2$]. Protein-bound GST beads were washed with deamidation buffer, and GST-RTA(N) was eluted with rehydration buffer (8 M urea, 2 M thiourea, 2% CHAPS, 0.5% IPG buffer, and 0.002% bromophenol blue) at room temperature. Samples were then analyzed by two-dimensional gel electrophoresis and immunoblotting.

Table 1. Primers for qRT-PCR.

CAD	TACGTGTCTCTCGCTCCTTC	CTGAGGCACCTTTACTCCCA
CTPS1	AGCTTGGCAGAAGCTCTGTA	CCAACTGCATCCCTAAGCAC
CTPS2	AACCGAGGACCCTGTGAAAT	TCACTGCTAGTTGCATCCCA
GFPT1	ACGGGAGACAGATTGTGGAG	ATCAGGCAGCCGTTTCAATC
GFPT2	CTCATCGTGATTGGCTGTGG	GCAAACGTCATCCCTGAACA
GMPS	CAGAGAGTCAAAGCCTGCAC	ACCCTGCACACCTACAGTTT
NADSYN1	CACACGGTTCCCATGTCCTA	TGTGCAGAGGCCTCCATAAG
PFAS	CCAGGGAAAGGAAGTCCGAT	GTGGTTGCACCACTAAAGGG
PPAT	CGAGAGGAATGTGGCGTGTT	CCCACGAGTCCCAGAGTGAT
ASNS	TGCTGGCAGGATCAACTAGG	GTGTTGTGGTGCATGCCTAT
ASNSD	GGGCGGGACTAAAGGAACTA	GAAGCAAACCAGACTGCACA
ORF21	AATCAAGCACCTCCACAACC	GCAAACCGACTGGCAAAAAT
PAN	CCGCCGATTGTGGGTTGATT	TTTTGTTCTGCGGGCTTATGGAG
ORF57	TGCTCTTGGCCTTTGTCCTA	TGCACAAGCTGTGATGTTCC
ORF59	CTATGCCAGCGTCGAGTACA	GGAAGGCAGTGGAGACGTTA
K8	CAAGAGGCGACTACATAGAAA	GATCACATACTTCGGCCTTAAC
ORF75	TGGAGCTGTTTGTCTCCAAG	GTTGAGAAAGTGCTCTGCCA

Constructing recombinant KSHV using the iBAC system

Mutagenesis of iBAC16 was performed as previously described (*54*). Briefly, the Kan/I-Sce I cassette was amplified from plasmid pEPKan-S by PCR. The purified PCR fragment was electroporated into iBAC16-containing GS1783 cells. Recombined clones were selected at 32°C on LB plates containing chloramphenicol (34 μg/ml) and kanamycin (50 μg/ml). Correct clones were then identified by PCR and confirmed by sequencing. Positive clones were induced at 42°C and plated on LB plates containing 1% L-arabinose and chloramphenicol (34 μg/ml) for secondary recombination. Clones from secondary recombination that were kanamycin sensitive were then picked and confirmed by PCR and sequencing. iBAC DNA was isolated using the Large Construct Kit (Qiagen) and used to transfect SLK cells with Lipofectamine 3000 (Thermo Fisher Scientific). SLK/iBAC cells were selected with hygromycin and induced with doxycycline (1 μg/ml) without or with sodium butyrate (1 mM) to generate recombinant virus. The sequences of primers are shown in Table 2.

MS analysis

For identification of deamidation sites, kRTA was purified from 293T cells transfected with a plasmid containing FLAG-kRTA by one-step affinity chromatography using anti-FLAG M2 agarose. Purified kRTA was subjected to SDS-PAGE and Coomassie staining. Gel slices containing RTA were prepared for in-gel digestion. MS analysis was performed by the Taplin Mass Spectrometry Facility of Harvard Medical School and Poochon Scientific (Frederick, MD).

RTA modeling

To render RTA structure, we used the publicly available I-TASSER program (http://zhanglab.ccmb.med.umich.edu/I-TASSER) (*55*). Briefly, the RTA protein sequence was input into the I-TASSER server, which predicts two most likely structures of RTA. The alignment

Table 2. Primers for iBAC16-RTA construction.

Kan-RTA-37D-F	CGAACTGAAGGCCCAACTCTACCAGTGTGTGCTCCTTATAGATGACGCATACGAAACAATTAGGGATAACAGGGTAATCGATTTATTC
Kan-RTA-37D-R	TTAGGTCACTGGGATCGTAGATTGTTTCGTATGCGTCATCTATAAGGAGCACACACTGGTGCCAGTGTTACAACCAATTAACC
Kan-RTA-225D-F	GCCGCTGGAGATCATGACCAAGGGTCAGCTCGCCCCTGAAGACTTTTACAGCATCACCGGTAGGGATAACAGGGTAATCGATTTATTC
Kan-RTA-225D-R	GCCGGCGTTTCTCAGCAGAACCGGTGATGCTGTAAAAGTCTTCAGGGGCGAGCTGACCCTGCCAGTGTTACAACCAATTAACC
Kan-RTA-37Q-F	CGAACTGAAGGCCCAACTCTACCAGTGTGTGCTCCTTATACAAGACGCATACGAAACAATTAGGGATAACAGGGTAATCGATTTATTC
Kan-RTA-37Q-R	TTAGGTCACTGGGATCGTAGATTGTTTCGTATGCGTCTTGTATAAGGAGCACACACTGGTGCCAGTGTTACAACCAATTAACC

of RTA with transcription factors of known structure suggests that model 1 (as shown in Fig. 4A) was the most likely folding of RTA. Subsequently, PyMOL was used to visualize the spatial position of the two deamidated sites (N37 and N225). The predicted NLS peptide sequence was highlighted to demonstrate the close proximity between the deamidation sites and the NLS sequence.

Statistical analysis

Statistical analysis was performed using unpaired two-tailed Student's *t* test. A *P* value of less than 0.05 is considered statistically significant. $*P < 0.05$, $**P < 0.01$, and $***P < 0.001$. Measurements were taken from distinct samples, and experiments were repeated independently at least three times. Results are expressed as the median ± SD.

SUPPLEMENTARY MATERIALS

Supplementary material for this article is available at http://advances.sciencemag.org/cgi/content/full/5/10/eaaw7373/DC1

Fig. S1. Cellular glutamine amidotransferases in KSHV lytic replication.
Fig. S2. PFAS restricts KSHV lytic replication.
Fig. S3. PFAS deamidates RTA.
Fig. S4. Deamidated RTA is impaired to activate KSHV lytic gene expression.
Fig. S5. Deamidation-resistant RTA-Q37 more potently induces KSHV lytic replication.
Fig. S6. Deamidation impairs RTA binding to importin.
Fig. S7. PFAS deamidates RTAs of other gamma herpesviruses.
View/request a protocol for this paper from *Bio-protocol*.

REFERENCES AND NOTES

1. V. G. Bhoj, Z. J. Chen, Ubiquitylation in innate and adaptive immunity. *Nature* **458**, 430–437 (2009).
2. K. M. Harlen, L. S. Churchman, The code and beyond: Transcription regulation by the RNA polymerase II carboxy-terminal domain. *Nat. Rev. Mol. Cell Biol.* **18**, 263–273 (2017).
3. N. E. Hynes, P. W. Ingham, W. A. Lim, C. J. Marshall, J. Massagué, T. Pawson, Signalling change: Signal transduction through the decades. *Nat. Rev. Mol. Cell Biol.* **14**, 393–398 (2013).
4. P. Tessarz, T. Kouzarides, Histone core modifications regulating nucleosome structure and dynamics. *Nat. Rev. Mol. Cell Biol.* **15**, 703–708 (2014).
5. M. J. Mycek, H. Waelsch, The enzymatic deamidation of proteins. *J. Biol. Chem.* **235**, 3513 (1960).
6. H. T. Wright, Nonenzymatic deamidation of asparaginyl and glutaminyl residues in protein. *Crit. Rev. Biochem. Mol. Biol.* **26**, 1–52 (1991).
7. J. Cui, Q. Yao, S. Li, X. Ding, Q. Lu, H. Mao, L. Liu, N. Zheng, S. Chen, F. Shao, Glutamine deamidation and dysfunction of ubiquitin/NEDD8 induced by a bacterial effector family. *Science* **329**, 1215–1218 (2010).
8. T. Sanada, M. Kim, H. Mimuro, M. Suzuki, M. Ogawa, A. Oyama, H. Ashida, T. Kobayashi, T. Koyama, S. Nagai, Y. Shibata, J. Gohda, J.-i. Inoue, T. Mizushima, C. Sasakawa, The *Shigella flexneri* effector OspI deamidates UBC13 to dampen the inflammatory response. *Nature* **483**, 623–626 (2012).
9. S. He, J. Zhao, S. Song, X. He, A. Minassian, Y. Zhou, J. Zhang, K. Brulois, Y. Wang, J. Cabo, E. Zandi, C. Liang, J. U. Jung, X. Zhang, P. Feng, Viral pseudo-enzymes activate RIG-I via deamidation to evade cytokine production. *Mol. Cell* **58**, 134–146 (2015).
10. J. Zhao, Y. Zeng, S. Xu, J. Chen, G. Shen, C. Yu, D. Knipe, W. Yuan, J. Peng, W. Xu, C. Zhang, Z. Xia, P. Feng, A viral deamidase targets the helicase domain of RIG-I to block RNA-induced activation. *Cell Host Microbe* **20**, 770–784 (2016).
11. P. S. Moore, Y. Chang, Kaposi's sarcoma–associated herpesvirus immunoevasion and tumorigenesis: Two sides of the same coin? *Annu. Rev. Microbiol.* **57**, 609–639 (2003).
12. J. Soulier, L. Grollet, E. Oksenhendler, P. Cacoub, D. Cazals-Hatem, P. Babinet, M. F. d'Agay, J. P. Clauvel, M. Raphael, L. Degos, F. Sigaux, Kaposi's sarcoma-associated herpesvirus-like DNA sequences in multicentric Castleman's disease. *Blood* **86**, 1276–1280 (1995).
13. R. G. Nador, E. Cesarman, D. M. Knowles, J. W. Said, Herpes-like DNA sequences in a body-cavity–based lymphoma in an HIV-negative patient. *N. Engl. J. Med.* **333**, 943 (1995).
14. S. J. Gao, L. Kingsley, D. R. Hoover, T. J. Spira, C. R. Rinaldo, A. Saah, J. Phair, R. Detels, P. Parry, Y. Chang, P. S. Moore, Seroconversion to antibodies against Kaposi's sarcoma–associated herpesvirus–related latent nuclear antigens before the development of Kaposi's sarcoma. *N. Engl. J. Med.* **335**, 233–241 (1996).
15. F. Massière, M.-A. Badet-Denisot, The mechanism of glutamine-dependent amidotransferases. *Cell. Mol. Life Sci.* **54**, 205–222 (1998).
16. X. Huang, H. M. Holden, F. M. Raushel, Channeling of substrates and intermediates in enzyme-catalyzed reactions. *Annu. Rev. Biochem.* **70**, 149–180 (2001).
17. M. R. Staudt, D. P. Dittmer, The Rta/Orf50 transactivator proteins of the gamma-herpesviridae. *Curr. Top. Microbiol. Immunol.* **312**, 71–100 (2007).
18. J. Myoung, D. Ganem, Generation of a doxycycline-inducible KSHV producer cell line of endothelial origin: Maintenance of tight latency with efficient reactivation upon induction. *J. Virol. Methods* **174**, 12–21 (2011).
19. J. Vieira, P. M. O'Hearn, Use of the red fluorescent protein as a marker of Kaposi's sarcoma-associated herpesvirus lytic gene expression. *Virology* **325**, 225–240 (2004).
20. D. Gong, N. C. Wu, Y. Xie, J. Feng, L. Tong, K. F. Brulois, H. Luan, Y. Du, J. U. Jung, C.-y. Wang, M. K. Kang, N.-H. Park, R. Sun, T.-T. Wu, Kaposi's sarcoma-associated herpesvirus ORF18 and ORF30 are essential for late gene expression during lytic replication. *J. Virol.* **88**, 11369–11382 (2014).
21. K. M. Duus, V. Lentchitsky, T. Wagenaar, C. Grose, J. Webster-Cyriaque, Wild-type Kaposi's sarcoma-associated herpesvirus isolated from the oropharynx of immune-competent individuals has tropism for cultured oral epithelial cells. *J. Virol.* **78**, 4074–4084 (2004).
22. D. Avey, S. Tepper, W. Li, Z. Turpin, F. Zhu, Phosphoproteomic analysis of KSHV-infected cells reveals roles of ORF45-activated RSK during lytic replication. *PLOS Pathog.* **11**, e1004993 (2015).
23. C. M. Sheridan, E. K. Heist, C. R. Beals, G. R. Crabtree, P. Gardner, Protein kinase A negatively modulates the nuclear accumulation of NF-ATc1 by priming for subsequent phosphorylation by glycogen synthase kinase-3. *J. Biol. Chem.* **277**, 48664–48676 (2002).
24. M. Soniat, Y. M. Chook, Nuclear localization signals for four distinct karyopherin-β nuclear import systems. *Biochem. J.* **468**, 353–362 (2015).
25. D. Görlich, U. Kutay, Transport between the cell nucleus and the cytoplasm. *Annu. Rev. Cell Dev. Biol.* **15**, 607–660 (1999).
26. Y. M. Chook, G. Blobel, Karyopherins and nuclear import. *Curr. Opin. Struct. Biol.* **11**, 703–715 (2001).
27. K. Lott, G. Cingolani, The importin β binding domain as a master regulator of nucleocytoplasmic transport. *Biochim. Biophys. Acta* **1813**, 1578–1592 (2011).
28. Y. Miyamoto, K. Yamada, Y. Yoneda, Importin α: A key molecule in nuclear transport and non-transport functions. *J. Biochem.* **160**, 69–75 (2016).
29. S. Kosugi, M. Hasebe, T. Entani, S. Takayama, M. Tomita, H. Yanagawa, Design of peptide inhibitors for the importin α/β nuclear import pathway by activity-based profiling. *Chem. Biol.* **15**, 940–949, 949 (2008).
30. A. E. Cansizoglu, B. J. Lee, Z. C. Zhang, B. M. A. Fontoura, Y. M. Chook, Structure-based design of a pathway-specific nuclear import inhibitor. *Nat. Struct. Mol. Biol.* **14**, 452–454 (2007).
31. J. T. West, C. Wood, The role of Kaposi's sarcoma-associated herpesvirus/human herpesvirus-8 regulator of transcription activation (RTA) in control of gene expression. *Oncogene* **22**, 5150–5163 (2003).
32. B. Damania, J. H. Jeong, B. S. Bowser, S. M. DeWire, M. R. Staudt, D. P. Dittmer, Comparison of the Rta/Orf50 transactivator proteins of gamma-2-herpesviruses. *J. Virol.* **78**, 5491–5499 (2004).
33. T. Ragoczy, L. Heston, G. Miller, The Epstein-Barr virus Rta protein activates lytic cycle genes and can disrupt latency in B lymphocytes. *J. Virol.* **72**, 7978–7984 (1998).
34. J. Munger, S. U. Bajad, H. A. Coller, T. Shenk, J. D. Rabinowitz, Dynamics of the cellular metabolome during human cytomegalovirus infection. *PLOS Pathog.* **2**, e132 (2006).
35. C. M. Goodwin, S. Xu, J. Munger, Stealing the keys to the kitchen: Viral manipulation of the host cell metabolic network. *Trends Microbiol.* **23**, 789–798 (2015).
36. E. L. Sanchez, T. H. Pulliam, T. A. Dimaio, A. B. Thalhofer, T. Delgado, M. Lagunoff, Glycolysis, glutaminolysis, and fatty acid synthesis are required for distinct stages of Kaposi's sarcoma-associated herpesvirus lytic replication. *J. Virol.* **91**, e02237-16 (2017).
37. Y. M. Chook, K. E. Süel, Nuclear import by karyopherin-βs: Recognition and inhibition. *Biochim. Biophys. Acta* **1813**, 1593–1606 (2011).
38. L. Twyffels, C. Gueydan, V. Kruys, Transportin-1 and Transportin-2: Protein nuclear import and beyond. *FEBS Lett.* **588**, 1857–1868 (2014).
39. D. Dormann, T. Madl, C. F. Valori, E. Bentmann, S. Tahirovic, C. Abou-Ajram, E. Kremmer, O. Ansorge, I. R. A. Mackenzie, M. Neumann, C. Haass, Arginine methylation next to the PY-NLS modulates Transportin binding and nuclear import of FUS. *EMBO J.* **31**, 4258–4275 (2012).
40. K. Fronz, S. Güttinger, K. Burkert, U. Kühn, N. Stöhr, A. Schierhorn, E. Wahle, Arginine methylation of the nuclear poly(a) binding protein weakens the interaction with its nuclear import receptor, transportin. *J. Biol. Chem.* **286**, 32986–32994 (2011).
41. M. T. Bedford, S. G. Clarke, Protein arginine methylation in mammals: Who, what, and why. *Mol. Cell* **33**, 1–13 (2009).
42. H.-S. Chen, P. Wikramasinghe, L. Showe, P. M. Lieberman, Cohesins repress Kaposi's sarcoma-associated herpesvirus immediate early gene transcription during latency. *J. Virol.* **86**, 9454–9464 (2012).
43. S. H. Speck, D. Ganem, Viral latency and its regulation: Lessons from the γ-herpesviruses. *Cell Host Microbe* **8**, 100–115 (2010).
44. Y. Yu, S. E. Wang, G. S. Hayward, The KSHV immediate-early transcription factor RTA encodes ubiquitin E3 ligase activity that targets IRF7 for proteosome-mediated degradation. *Immunity* **22**, 59–70 (2005).

45. Y. Gwack, H. Nakamura, S. H. Lee, J. Souvlis, J. T. Yustein, S. Gygi, H.-J. Kung, J. U. Jung, Poly(ADP-ribose) polymerase 1 and Ste20-like kinase hKFC act as transcriptional repressors for gamma-2 herpesvirus lytic replication. *Mol. Cell. Biol.* **23**, 8282–8294 (2003).
46. Y. Izumiya, K. Kobayashi, K. Y. Kim, M. Pochampalli, C. Izumiya, B. Shevchenko, D.-H. Wang, S. B. Huerta, A. Martinez, M. Campbell, H.-J. Kung, Kaposi's sarcoma-associated herpesvirus K-Rta exhibits SUMO-targeting ubiquitin ligase (STUbL) like activity and is essential for viral reactivation. *PLOS Pathog.* **9**, e1003506 (2013).
47. J. Guito, A. Gavina, D. Palmeri, D. M. Lukac, The cellular peptidyl-prolyl *cis/trans* isomerase Pin1 regulates reactivation of Kaposi's sarcoma-associated herpesvirus from latency. *J. Virol.* **88**, 547–558 (2014).
48. Y. Liang, J. Chang, S. J. Lynch, D. M. Lukac, D. Ganem, The lytic switch protein of KSHV activates gene expression via functional interaction with RBP-Jκ (CSL), the target of the Notch signaling pathway. *Genes Dev.* **16**, 1977–1989 (2002).
49. Z. Yang, C. Wood, The transcriptional repressor K-RBP modulates RTA-mediated transactivation and lytic replication of Kaposi's sarcoma-associated herpesvirus. *J. Virol.* **81**, 6294–6306 (2007).
50. A. N. Lane, T. W.-M. Fan, Regulation of mammalian nucleotide metabolism and biosynthesis. *Nucleic Acids Res.* **43**, 2466–2485 (2015).
51. Z. He, Y. Liu, D. Liang, Z. Wang, E. S. Robertson, K. Lan, Cellular corepressor TLE2 inhibits replication-and-transcription- activator-mediated transactivation and lytic reactivation of Kaposi's sarcoma-associated herpesvirus. *J. Virol.* **84**, 2047–2062 (2010).
52. R. E. Means, S. Ishido, X. Alvarez, J. U. Jung, Multiple endocytic trafficking pathways of MHC class I molecules induced by a Herpesvirus protein. *EMBO J.* **21**, 1638–1649 (2002).
53. H. Feng, X. Dong, A. Negaard, P. Feng, Kaposi's sarcoma-associated herpesvirus K7 induces viral G protein-coupled receptor degradation and reduces its tumorigenicity. *PLOS Pathog.* **4**, e1000157 (2008).
54. B. K. Tischer, G. A. Smith, N. Osterrieder, *En passant* mutagenesis: A two step markerless red recombination system. *Methods Mol. Biol.* **634**, 421–430 (2010).
55. Y. Zhang, I-TASSER server for protein 3D structure prediction. *BMC Bioinformatics* **9**, 40 (2008).

Acknowledgments: We thank B. Damania, A. Whitehouse, and E. Johannsen for providing RTA plasmids. We thank J. Wu and F. Zhu for providing the KSHV iBAC and iSLK/rKSHV.219 system, Y. Izumiya for anti-RTA serum, J. Jung for anti-K3 serum, R. Sun and T. Wu for HOKs, and J. Hao (Poochon Scientific) and S. Gygi and R. Tamaino (Taplin Mass Spectrometry, Harvard Medical School) for MS analyses. We thank R. Amatya for professional editing of the manuscript. **Funding:** This work was supported by grants from the NIH (DE027557, DE026003, CA221521, AI134105, and CA180779). **Author contributions:** J.L. and P.F. conceived the study. J.L., J. Zhao, S.X., S.Z., J. Zhang, J.X., R.G., M.T., Y.Z., V.T., K. Lee and K. Lan performed experiments and/or contributed reagents. J.L., J. Zhao, S.X., V.T., H.F., and P.F. analyzed the data. J.L. and P.F. wrote the paper, with input from all authors. **Competing interests:** The authors declare that they have no competing interests. **Data and materials availability:** All the data needed to evaluate the conclusions in this paper are present in the paper and/or the Supplementary Materials. Additional data related to this paper may be requested from the authors.

Submitted 20 January 2019
Accepted 14 September 2019
Published 9 October 2019
10.1126/sciadv.aaw7373

Citation: J. Li, J. Zhao, S. Xu, S. Zhang, J. Zhang, J. Xiao, R. Gao, M. Tian, Y. Zeng, K. Lee, V. Tarakanova, K. Lan, H. Feng, P. Feng, Antiviral activity of a purine synthesis enzyme reveals a key role of deamidation in regulating protein nuclear import. *Sci. Adv.* **5**, eaaw7373 (2019).